Periodic instationarities of granular flows in conical hoppers

Guilhem Mollon

Periodic instationarities of granular flows in conical hoppers

Guilhem Mollon[1]

Abstract
Granular flows through converging sections such as conical hoppers have been reported to be submitted to instationarities, which in certain circumstances can appear to be organized and periodic. In this paper, we explore this phenomenon by conducting discrete element modelling simulations of a 3D gravity-driven hopper flow and varying a large number of parameters such as hopper geometry and granular sample properties. Dedicated postprocessing techniques are developed and used to investigate the spatial and temporal patterns of these instationarities and to bring some understanding on the physics of this spontaneous phenomenon. Numerical results show that a clear structure appears for these instationarities, under the form of rapidly propagating waves relating variations in velocity magnitude and coordination number. While very faint, periodic variations of the sample density are also detected. The parametric study reveals that the self-organization of these variations requires a narrow set of conditions in terms of hopper geometry and intergranular contact friction coefficient.

Keywords Granular flow · Periodic variations · Hopper flow · DEM

1 Introduction

Hopper flow is a common problem in physics of granular flows [1]. It consists in the gravity-driven flow of a granular assembly through a converging channel, and the classic hourglass problem is a good example of this class of situations. Besides its theoretical interest, this problem also has a large number of practical applications since converging flows are used in a wide variety of industries manipulating powders and grains [2–5]. It has therefore attracted a large attention from the scientific community, both from the practical and academic viewpoints. Theoretical [6–9], experimental [10–17] and numerical [18–22] studies have been reported using a number of different tools.

The most common quantity of interest that is extracted from such studies is the hopper discharge rate, i.e. the amount of matter passing through the hopper outlet in a certain amount of time. Contemporary studies use the hopper flow configuration to investigate such complex topics as avalanching [23], self-structuration of the granular fabric triggered by the converging flow [24], shape-induced flow regimes [25], or phase change (i.e. jamming) of the granular sample [26]. Despite the simplicity of its geometry, the hopper flow gives rise to fairly complex behaviors, and one of the most mysterious is the spontaneous emergence of periodic flow instationarities. Such instationarities, sometimes called fluctuations, have been reported experimentally [11, 13, 14, 16] and numerically [18, 20, 22].

In particular, a numerical study accounting for realistic sand grains shapes but limited to 2D kinematics [20] showed that these periodic instationarities could be described as waves propagating upstream, triggered by the build-up of force chains from the hopper walls. In the present study, we enrich this numerical framework by adding a third dimension and deploying appropriate statistical methods to extract knowledge on this phenomenon. Section 2 presents the numerical framework, including the postprocessing techniques, and describes the main flow parameters for a reference case. Section 3 provides a detailed analysis of the instationarities detected for this reference case, and Sect. 4 adds a parametric study involving a large number of simulations and systematically investigating several parameters of the system. Discussion of the results and proposals for future research avenues are presented in Sect. 5.

✉ Guilhem Mollon
guilhem.mollon@insa-lyon.fr

[1] Université de Lyon, LaMCoS, INSA-Lyon, CNRS UMR5259, 69621 Villeurbanne, France

2 Numerical framework

2.1 Simulations principles and parameters

The Discrete Element Method (DEM, [27]) has now become a very common investigation tool in granular science, both for academics and practitioners, and is used in a large variety of scientific fields such as geophysics [28] or tribology [29]. It is based on an explicit integration in time of the Newtonian dynamics of each one of the bodies composing the granular assembly. In addition to a possible gravity field, these bodies are submitted to interaction forces that arise when they enter into contact with each other. Various phenomenological contact laws can be used, but we will stick in the present study to the standard contact model of DEM. It includes contact stiffnesses in the normal (k_n) and tangential (k_t) directions, which can be seen either as purely numerical regularization parameters or as a proxy for the local deformations of the contacting bodies. In the latter case, non-linear stiffnesses reproducing Hetrz–Mindlin theory can be used. In the present study, however we remain in the first interpretation of these parameters, and use $k_n = k_t = constant$. The standard model also includes two modes of energy dissipation: a classical dashpot introducing a damping γ in the normal direction, and a Coulomb friction coefficient μ in the tangential direction.

In this paper we perform DEM simulations of perfectly conical hopper discharge, with various sample properties and hopper geometries. All the granular samples are composed of 50,000 spherical grains with a mean diameter $D = 1$. Since the study is dimensionless, this quantity will be used as a length unit. The size distribution of the grains around this mean value is homogeneous, with coefficients of variation COV_D (i.e. ratio of the standard deviation to the mean value) of D varying from 0% (perfectly monodisperse sample) to 80% (strongly polydisperse sample). The opening diameter L of the hopper varies between $6D$ and $14D$, and the hopper angle to the horizontal α varies from 40° to 80° (Fig. 1). The gravity is kept constant and equal to 10, and the density of the grains is equal to 1. Hence, a given simulation is defined by 6 parameters, and the reference simulation corresponds to $COV_D = 40\%$, $L = 10D$, $\alpha = 70°$, $k_n = 10^5$, $\mu = 0.4$, and $\gamma = 0.2$. The results of this simulation are detailed in the next section. The time step is constant and equal to 10^{-5} *time units* for all the simulations reported here. The only characteristic times of the system are related to free fall and to single-grain harmonic oscillations, and are respectively equal to:

$$T_g = \sqrt{g/D} \approx 0.316$$

$$T_k = \sqrt{6k_n/\left(\pi D^3\right)} \approx 0.00229$$

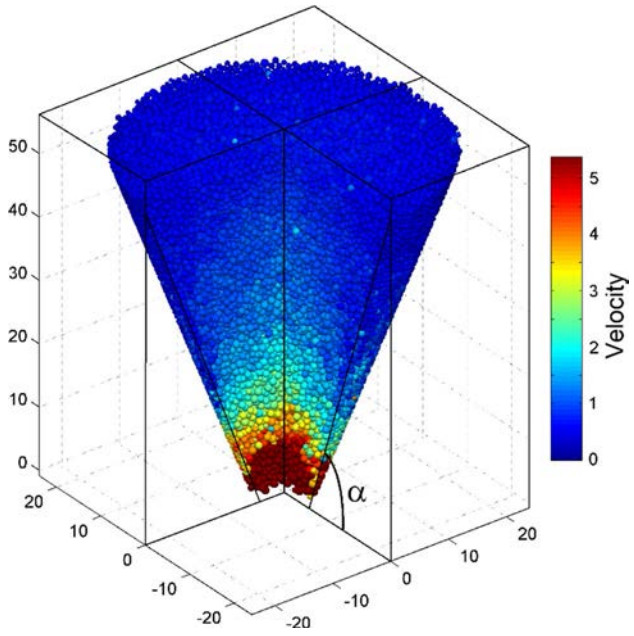

Fig. 1 Snapshot of particle velocities during hopper discharge

2.2 Postprocessing techniques

The main quantity of interest when studying hopper flow is the discharge rate, since it is of primary importance regarding the practical use of such a system for engineering applications. Figure 2 shows the evolution in time of the proportion of granular material passed through the hopper outlet, as predicted by the reference simulation. The passing rate is constant, in good agreement with existing theories and observations. This is also the case for all the other simulations described in this work.

Since this paper is primarily interested in granular flow instationarities, a dedicated postprocessing technique is needed in order to follow the evolution of quantities which vary both in space and time. First, in order to avoid a drift in the average values of local flow parameters, the focus is put on a short time interval used as an observation window. As shown in Fig. 2, this interval runs from 5 to 7 time units after opening of the hopper, in order to make sure that the discharge flow has reached a steady state (in some simulations described in the next sections, a different starting time was chosen for the same reason). This time interval is short enough to consider that the mean flow parameters do not change much, but long enough to observe a statistically significant number of fluctuations.

A major difficulty is the fact that relevant quantities are attached either to one grain (velocity and coordination number, i.e. number of contacting neighbors) or to a collection of grains (solid fraction). This is a logical consequence of

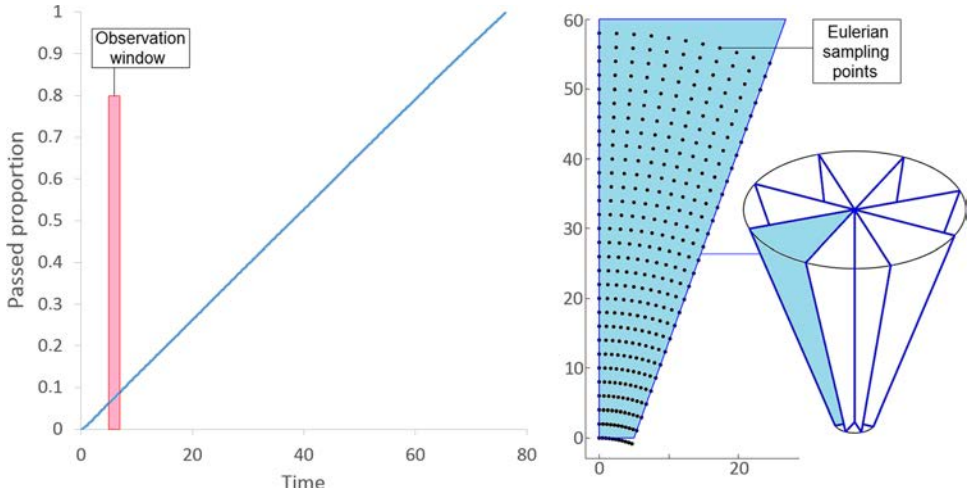

Fig. 2 Left: Proportion of passed material in time in the reference simulation, and time-window used for the observation of flow instationarities; right: 3D Eulerian grid used to map flow parameters in time

the Lagrangian framework used to describe the problem, but renders direct interpretations difficult because these grains (or groups of grains) are in constant motion. This issue was already tackled in several papers with various mathematical approaches [30, 31]. In this paper, a specific technique is used in order to transfer these quantities to fixed coordinates and study the flow from an Eulerian perspective. Grain-attached quantities (velocity and coordination number) are interpolated at fixed locations between grains using moving least squares [32], in a spherical radius equal to 5 distance units around the desired location (it is important to notice that a certain amount of spatial averaging is included in the process). And a local solid fraction at a given fixed location (x, y, z) of space is computed by a weighted averaging technique which complies with the principle of mass conservation:

$$F_s(x, y, z) = \left(\pi d^2\right)^{3/2} \cdot \sum V_i e^{-r_i(x,y,z)/d}$$

In this expression, V_i corresponds to the volume of the grain i, $r_i(x, y, z)$ corresponds to the distance from the center of this grain to the location (x, y, z), and the summation is executed on all the grains i located in a sphere of radius $d = 8D$ around this location, which thus controls the cut-off interpolation distance. These post-processing techniques are used to extract and analyze the evolutions of velocity, coordination number and solid fraction at various locations, with a time step of 0.002 time units. A 3D Eulerian grid is used for that purpose, as shown in Fig. 2: 330 points are defined in a given vertical half-plane containing the symmetry axis of the hopper, and 8 such half-planes are used in order to cover the whole system.

2.3 Mean fields

Average fields of vertical and radial velocities, of coordination number and of solid fraction are plotted in Fig. 3 (in one half-plane, after averaging in the circumferential direction), as well as the corresponding time-related standard deviations of these quantities, for the reference simulation. In terms of time-average, the radial component of the velocity field is small compared to the vertical one, which progressively increases in norm when getting closer to the hopper outlet. The coordination number and the solid fraction are almost constant in the hopper (close to 3.5 and 0.45 respectively), except in the neighborhood of the inlet and of the outlet of the hopper where these values drop because of reduced local confining stress. These behaviors are consistent with common hopper flow observations (e.g. [16, 20]).

The time-variability of the velocity field presents some interesting spatial patterns. Two areas are observed where velocity has important variations in time: the area located close to the outlet (because of local agitation related to the change of flow regime when the grains are released from the hopper confinement) and a broad area located in the upper half of the hopper, starting about $25 - 30D$ above the outlet and extending up to the inlet. There is also a large time variability of the coordination number in the same area, while the solid fraction variability is very low in the whole sample.

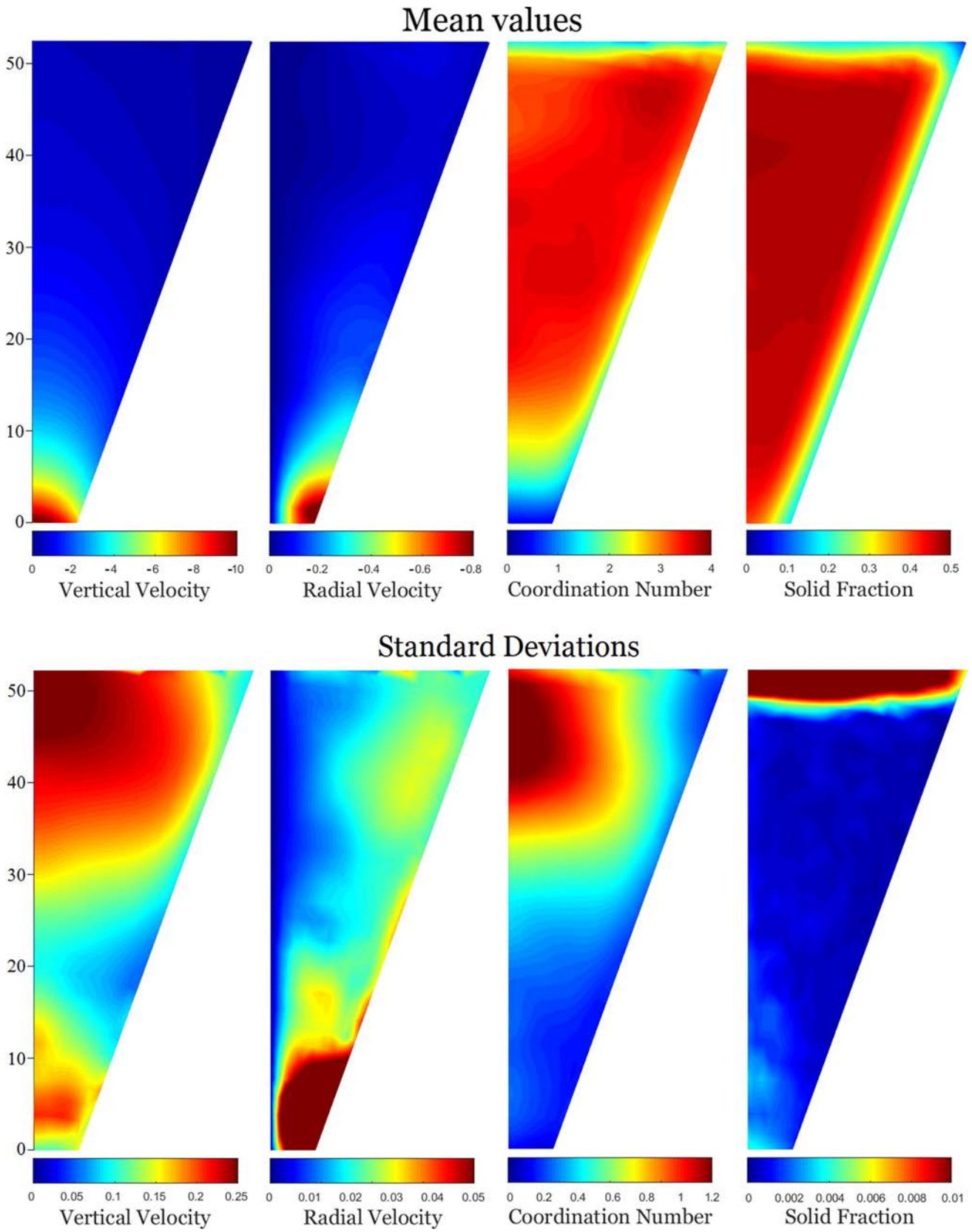

Fig. 3 Local mean values and standard deviations (related to local variations in time) of flow parameters during the observation window for the reference experiment

3 Analysis of the instationarities

3.1 Detection

In order to describe quantitatively the flow instationarities, we perform the same postprocessing approach on a vertical profile corresponding to the axis of revolution of the hopper, in the reference case. The sampling time-step remains equal to 0.002 time units, and the sampling step in space along the vertical axis is equal to $0.01D$. We therefore obtain data under the form $Q(t, Y)$ where Q is velocity magnitude, coordination number, or solid fraction, and where t and Y denote time (with a zero corresponding by convention to the beginning of the observation time window, for the remainder of the present study) and vertical position (with a zero corresponding to the hopper outlet).

These data are represented as space–time diagrams in the left-hand column of Fig. 4. Some organized fluctuations clearly appear in the diagrams of velocity and coordination number (but not in the diagram of solid fraction). It is however difficult to read and quantify them, because they are superimposed to a mean field which is spatially varying (as well as its time-variability, as shown in Fig. 3). This is especially the case for the velocity, which progressively increases when getting closer to the outlet. For this reason, quantities are locally normalized, using the following formula:

$$\tilde{Q}(t, Y) = \frac{Q(t, Y) - \mu_Q(Y)}{\sigma_Q(Y)}$$

In this expression, $\tilde{Q}(t, Y)$ is the normalized quantity, $Q(t, Y)$ is the initial quantity, $\mu_Q(Y)$ is the time-average of Q at the location Y, and $\sigma_Q(Y)$ is the corresponding time-related standard deviation. Normalized velocity, coordination number, and solid fraction are plotted on space–time diagrams on the right-hand column of Fig. 4. Fluctuation patterns are much clearer in that normalized form: for both velocity and coordination number, they take the form of periodic oscillations around the mean value, which seem to be strongly synchronized in the vertical directions. More precisely, the lower part of the hopper does not seem to be subjected to any organized pattern, but above a certain height (which is close to $Y = 15D$ for the velocity and $Y = 10D$ for the coordination number), fluctuations acquire a structure which remains the same up to the hopper inlet. The case of solid fraction is more complex: normalized solid fraction seems also to be submitted to periodic and synchronized oscillations in the upper part of the hopper, but these oscillations are fainter and are blurred by noisy descending patterns which may be related to the downward motion of undisturbed grains structures within the granular flow.

It is interesting to notice that the periods of oscillation of the three considered quantities are the same, indicating that these oscillations are part of the same physical phenomenon. In similar studies in 2D [16, 20], it was observed that such oscillations could be interpreted as waves emanating from the hopper outlet and travelling upwards in the hopper. The velocity of these waves was reported to be much greater than that of the flowing grains. This interpretation is debatable here since the oscillations described in Fig. 4 seem to be synchronized in space. At a first glance, indeed, they look like stationary oscillations and do not seem to exhibit any propagation pattern. However, this could be related to such waves travelling too fast (with respect to their time-period) for this propagation to be detectable visually, because the hopper is not high enough to allow for a sufficient propagation distance. A preliminary analysis of similar 3D simulations [22] indeed revealed that the use of a lower value of the contact stiffness between grains was able to reduce the period of the oscillations and to slow-down their propagation, allowing a clear observation of the wave upwards travel. We can thus hypothesize that the oscillations which are described here result from the same phenomenon than in 2D [20], but with waves travelling much faster.

3.2 Patterns in time

Figure 5 shows an illustrative snapshot of the spatial fields of normalized velocity and coordination number in a vertical plane of symmetry of the hopper. This visualization reveals that such instantaneous fields exhibit some clear trends (for example in the vertical direction) but an important spatial variability. Hence, the extraction of meaningful patterns requires some specific procedures.

For this purpose, we explore the autocorrelation structure of the time variations of the normalized quantities in Fig. 6. At a given location Y on the revolution axis of the hopper, a given quantity $Q(t, Y)$ varies in time, and its autocorrelation function $A_Q(\Delta t, Y)$ can be computed as a function of the phase shift Δt by computing the correlation between $Q(t, Y)$ and $Q(t + \Delta t, Y)$. Maps of this autocorrelation are plotted in Fig. 6 for velocity, coordination number, and solid fraction and reveal interesting patterns. For both velocity and coordination number, a very clear autocorrelation peak occurs for a phase shift $\Delta t = T = 0.192$ *time units*, indicating a strong periodicity. This is only the case, however, beyond a certain height above the hopper outlet (close to $Y = 15D$ for the velocity and $Y = 10D$ for the coordination number), in good accordance with the observations of Fig. 4. Below this height, the correlation structure disappears. Besides, a similar map of solid fraction does not show any clear autocorrelation peak, indicating that the faint periodic signal observed in Fig. 4 is not strong enough to be revealed by this procedure. It is interesting to notice that the measured

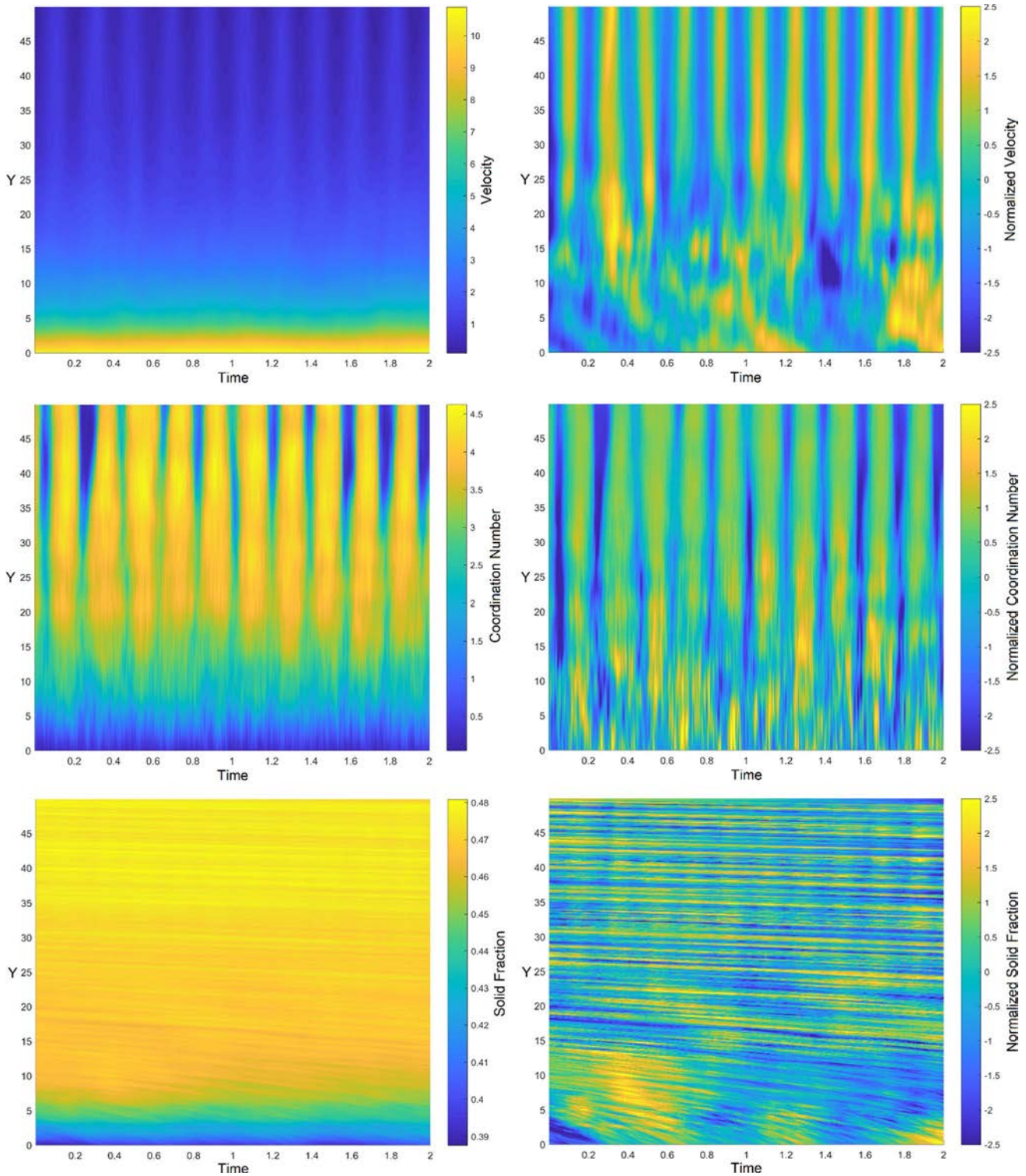

Fig. 4 Space-time diagram of the velocity magnitude, of the coordination number, and of the solid fraction, on the vertical revolution axis of the hopper; left: raw quantities; right: normalized quantities

period T is way larger than the single-grain oscillation characteristic time T_k, but of the same order of magnitude than the characteristic free-fall time T_g.

The lower-right corner of Fig. 6 shows profiles of autocorrelation for the three quantities, as a function of location Y for a phase shift $\Delta t = T = 0.192$ (confirming that the

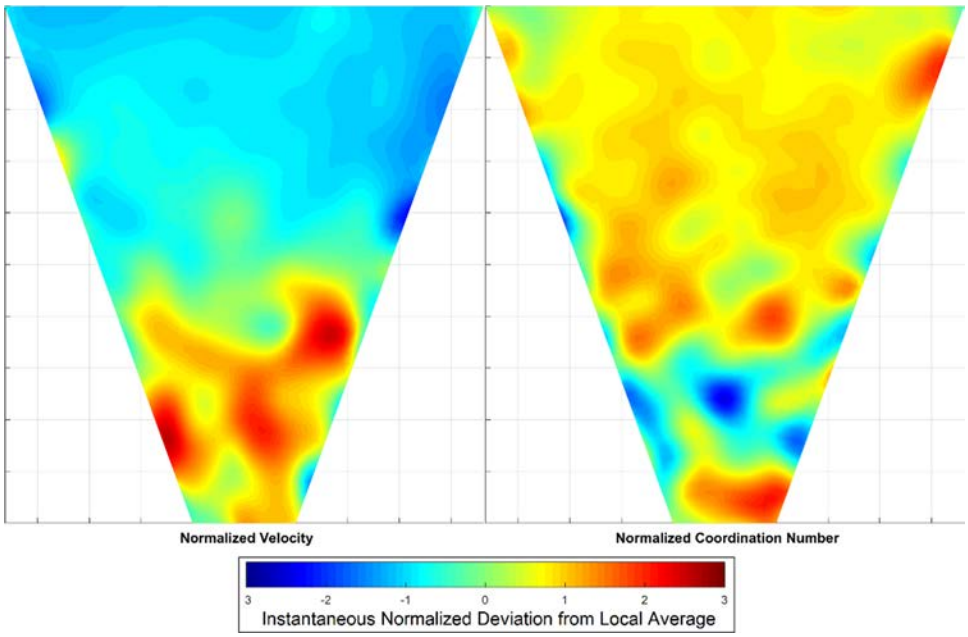

Fig. 5 Snapshot of normalized flow parameters in a symmetry plane of the hopper

coordination number signal acquires its T-periodicity at a lower height than velocity), and as a function of phase shift Δt for the location $Y = 42.5$ (showing that the autocorrelation peak is very close to 1 for the velocity signal, indicating a near-perfect periodicity).

In order to describe more precisely the waveform of the detected oscillations, we plot in Fig. 7 the evolution in time of the normalized velocity magnitude, coordination number, and solid fraction at selected illustrative locations. More specifically, we focus on eight different locations in the hopper which share the same Y-coordinate and the same distance to the hopper axis, but in eight different radial directions (corresponding to the eight half-planes described in Fig. 2). As expected, these signals are very well synchronized (over about ten periods) for velocity and coordination number but do not show any organized pattern for the solid fraction. These signals are then stacked (i.e. averaged on the 8 locations and on 10 successive periods, using the main period value $T = 0.192$ obtained in the previous paragraph), as is often done in seismology to de-noise earthquakes waveforms [33]. The purpose of this operation is to focus on the systematic variations of the quantities that follow the main oscillation period while getting rid (by averaging) of all the other non-systematic variations. The resulting waveforms are plotted in the lower-part of Fig. 7 for the three quantities (velocity, coordination number, and solid fraction). Two identical periods of this waveform are shown to ease the reading.

Several interesting observations can be extracted from these curves. It appears that the velocity oscillations are quasi-harmonic, with an evolution which is very symmetric around the average value (equal to 0 for such normalized quantities). The coordination number waveform, on the other hand, is strongly skewed and far from being harmonic. The main pattern that this quantity follows in time is divided in a rather long period of values moderately larger than the average (up to $+1$ standard deviation), followed by a shorter but stronger drop below the average (up to -2 standard deviations). The stacking operation also reveals a systematic evolution of the solid fraction which could not be inferred from autocorrelation patterns (Fig. 6) or from the raw time-signals (upper part of Fig. 7). While noisier than the other quantities, the waveform of the solid fraction is very clear, and consists in a symmetrical signal, somewhere between harmonic and triangular waveforms.

Solid fraction and coordination number waveforms are in phase, indicating that these two quantities are directly related. As could be expected, a larger solid fraction correlates with an increase in the number of contacts, and vice versa. Their waveforms are however different because of the intrinsically asymmetrical character of mechanical contacts. Indeed, since the stiffness of the contacts is pretty large, the interpenetration distance of contacting grains is always quite small. A minor decrease of the solid fraction is hence sufficient to increase a little bit the distance between the centers of the grains, which leads to the loss of a large number of contacts. Conversely, when the solid fraction increases, some contacts can be created if the initial gap separating the grains is small enough for them to eventually touch, but this situation is made rarer by the large stiffness of the contact model. This is the reason why the coordination number oscillations are skewed towards the low values while the solid fraction follows a more harmonic evolution.

In contrast, the waveforms of velocity and coordination number are shifted in time: the velocity oscillations are

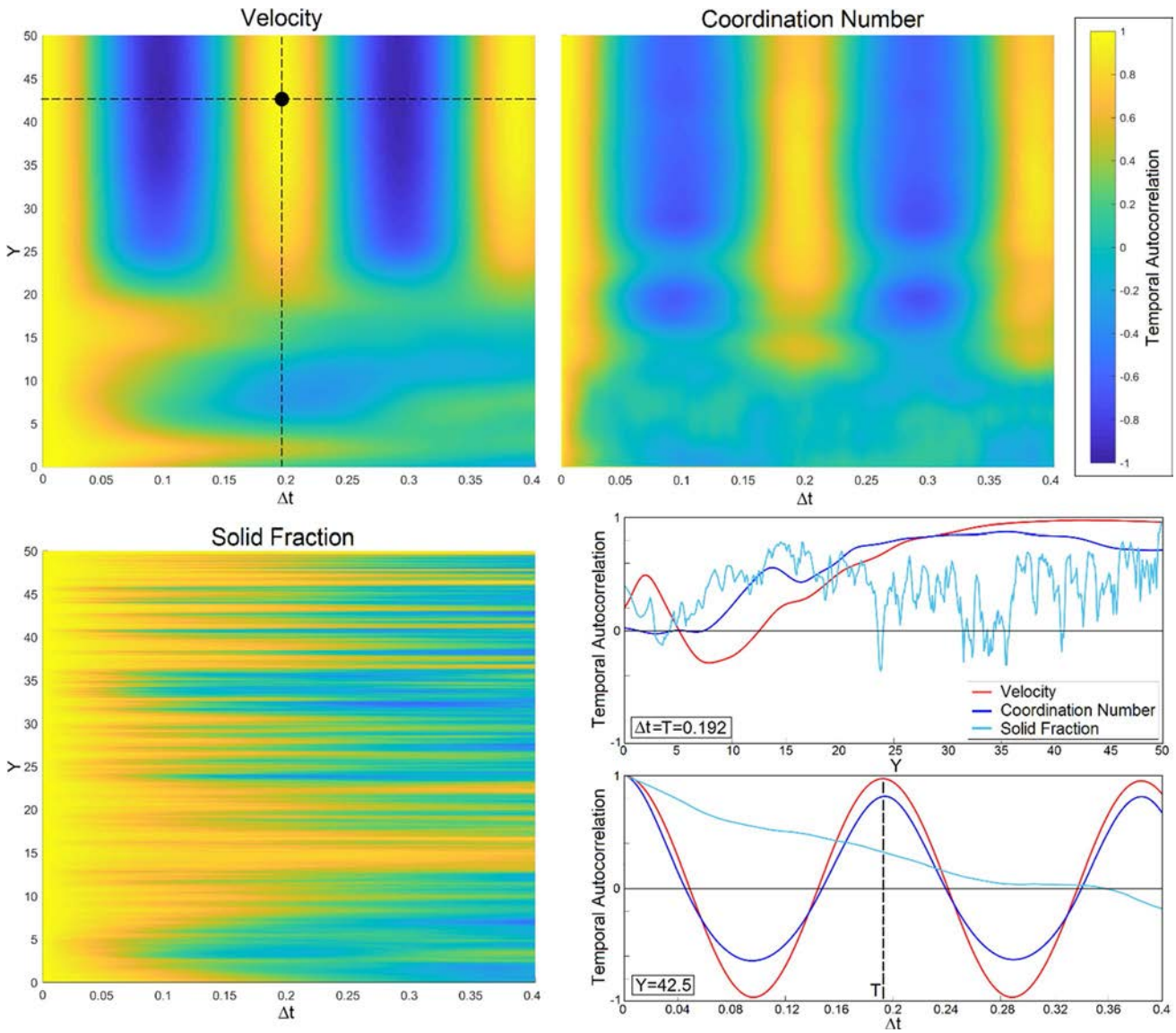

Fig. 6 Autocorrelation in time of normalized flow quantities on the revolution axis of the hopper, presented as functions of location Y and of phase shift; upper-left: Velocity autocorrelation map; upper-right: Coordination number autocorrelation map; lower-left: Solid fraction autocorrelation map; lower-right: autocorrelation profiles

delayed by about $0.3T$ with respect to the variations of coordination number. Broadly speaking, it appears that velocity magnitude decreases when the coordination number is above its average, and increases when it is below its average. Likewise, coordination number decreases when velocity is below its average, and increases when velocity is above its average.

3.3 Patterns in space

This stacking technique is further applied to all locations in the hopper half-plane in order to analyze the spatial patterns of evolution of the three quantities of interest, and the resulting fields are plotted for one period T in Fig. 8. The lower part of the hopper appears to have no significant variation in this representation. It does not mean that the fields do not vary in time at these locations, it means that staking the signals on a T-period averages them and thus that the signals do not have any T-periodicity in this area. The upper row of Fig. 8 shows that the velocity oscillations only appear above a height of about $15-20D$ (confirming the observations of Figs. 6 and 7), and that they are very homogeneous. This area can be described as the organized fluctuations area. The same observation applies to the coordination number, although it clearly appears that organized fluctuations do start at a lower height of $10-15D$, and that they are very slightly less homogeneous

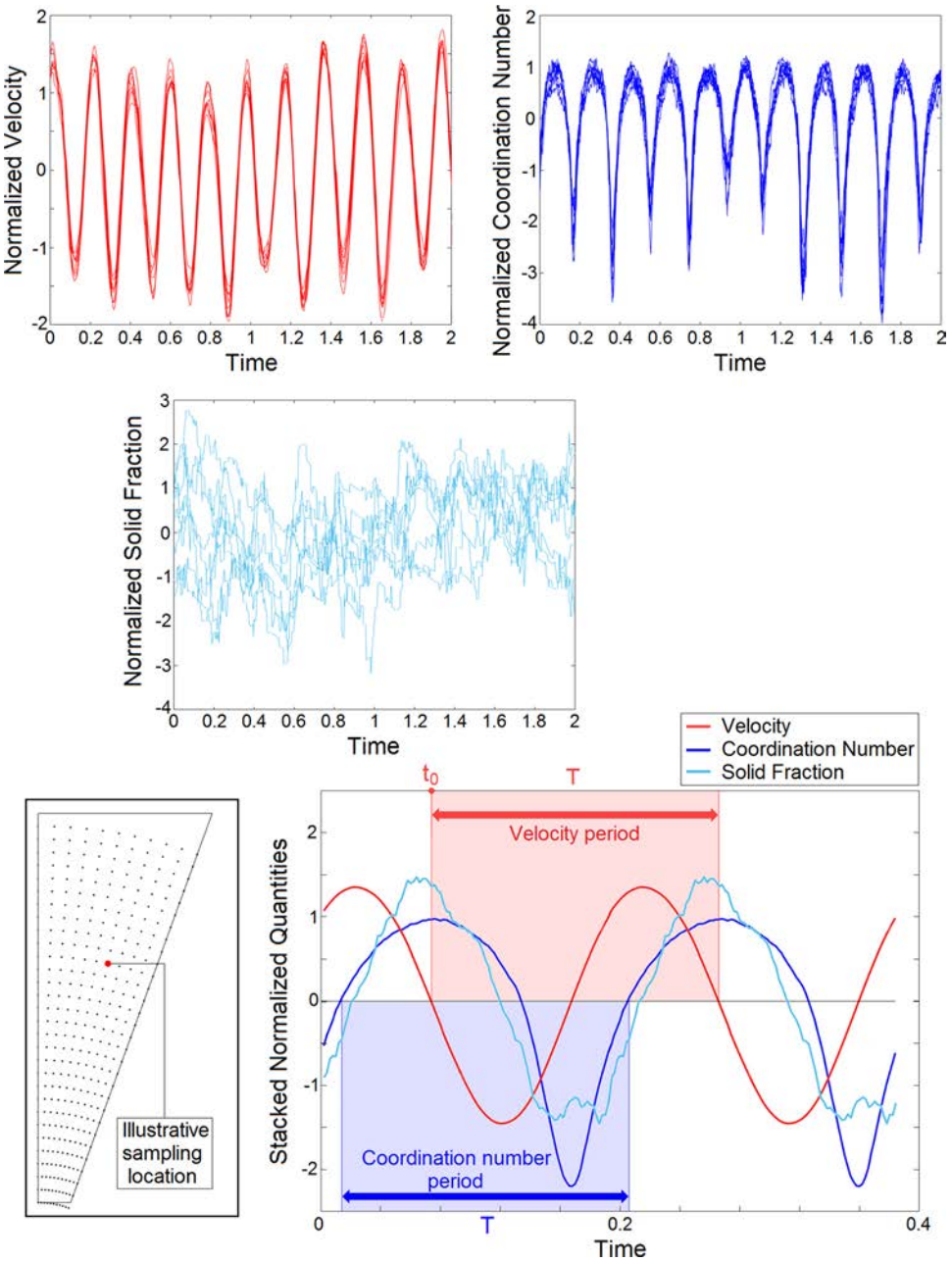

Fig. 7 Pattern extraction for the velocity, the coordination number, and the solid fraction, at an illustrative location in the hopper. Upper-part: time-signals of normalized quantities obtained on eight similar locations of the hopper (same height and distance to the axis, different radial directions as shown in Fig. 2); lower-part: stacked signals for the three quantities

in space. Periodic and organized variations of the solid fraction only occur in the upper part of the hopper but are less clearly defined (although easily observable in this representation) than for the two other quantities.

The patterns shown in Fig. 8 suggest synchronized oscillations instead of propagating waves, but do not allow to conclude. A closer view is brought by Fig. 9. The upper part of this figure provides plots of stacked signals of the normalized velocity magnitude at selected locations in the hopper. The left-hand curves focus on locations aligned vertically, and the right-hand curves focus on locations aligned radially. Stacked curves are slightly shifted vertically to enable comparison, and points of minimum, maximum, and zero normalized velocities are highlighted. It allows to infer the direction of propagation of the signal, and indicative arrows are added as a guide to the eye. This plot seems to indicate that the signals are more and more delayed when travelling upwards and inwards (radially-speaking).

This view is confirmed by the lower part of Fig. 9, which shows maps of wave delay, provided by the stacked signals at every locations of the half-plane. More specifically, it shows a map of the arrival time of the maximum velocity (lower-left part) and of the minimum velocity (lower-right part). The time delay between two successive lines in the maps is constant and equal to 0.0005 time units. It clearly appears that the velocity increase initiates

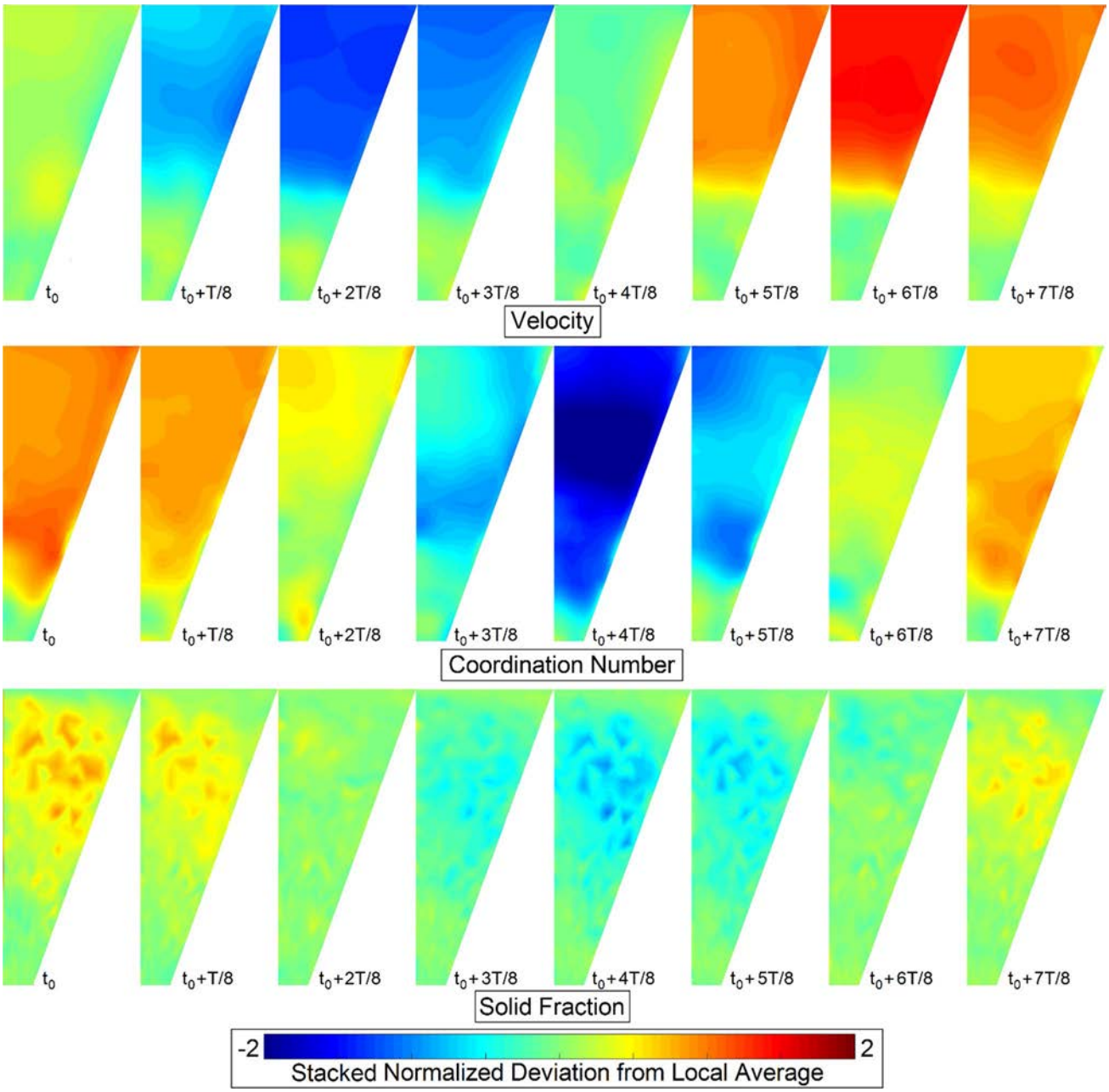

Fig. 8 A typical oscillation cycle of period T starting at time t_0 (Fig. 7), obtained by stacking for the three quantities of interest in a hopper half-plane

on the lateral wall of the hopper, propagates inwards, and then upwards. The velocity decrease, on the contrary, initiates at the walls but also at the inlet and below the organized oscillation area, and then propagates inwards. It also propagates about three times faster. These observations confirm that the detected instationarities are indeed waves propagating in the hopper, and not only stationary vibrations. In the considered geometry, the propagation time remains however very small when compared to the main period of the oscillations.

4 Parametric study

4.1 Influence of the particle size distribution

In this section, we investigate the influence of the size variability of the granular sample on the flow instationarities. This variability is quantified by the coefficient of variation of the particles diameters COV_D, i.e. the ratio of the standard deviation to the mean value of the diameter (which is always equal to 1 length unit in this study). COV_D takes the

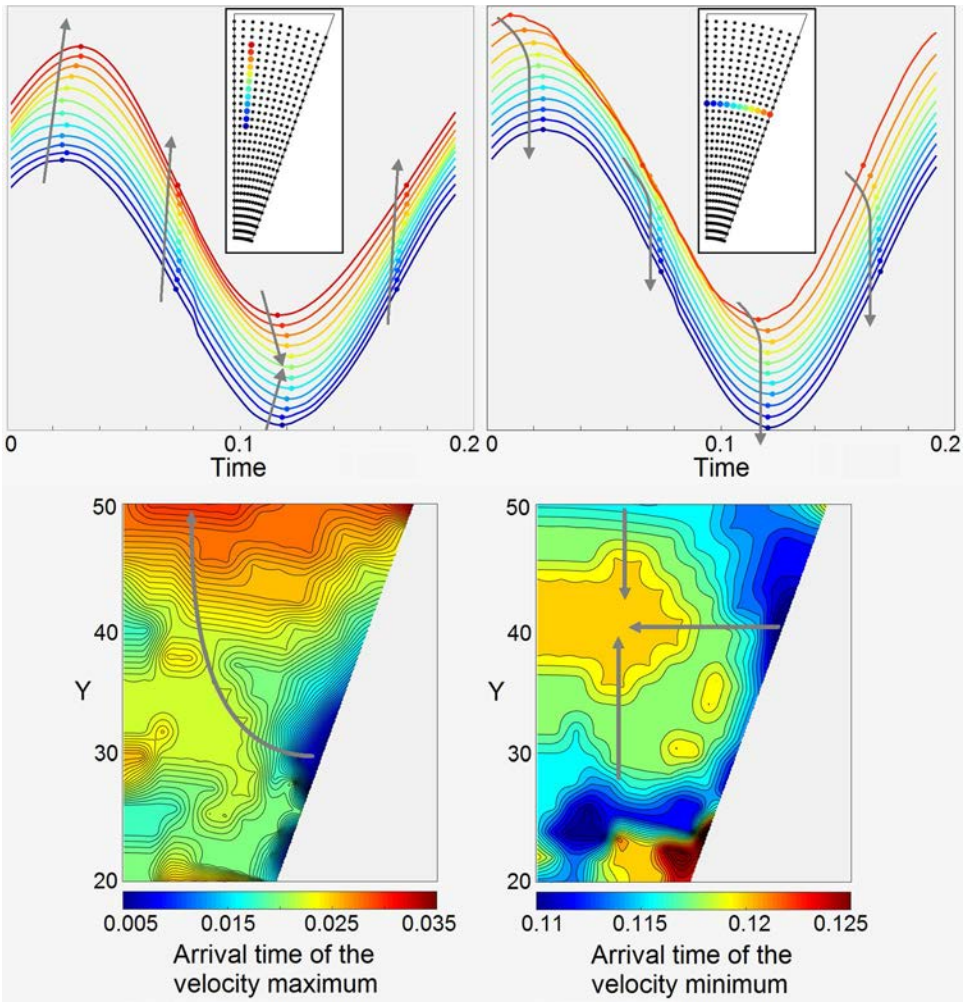

Fig. 9 Typical velocity signals (obtained by stacking) at several locations in a hopper half-plane (with a small vertical shift to ease the reading), maps of signal delays, and corresponding propagation directions; upper-left: stacked signals on a vertical profile; upper-right: stacked signals on a radial profile; lower-left: arrival time of the maximum of velocity; lower-right: arrival time of the minimum velocity

values 0%, 20%, 40% (reference case), 60%, and 80%, while all the other simulation parameters are kept constant and equal to those of the reference case. Results are presented in Fig. 10, and include (1) the discharge rate of the hopper flow during the whole discharge (this rate is found to be constant throughout the whole simulation, for all simulations presented in this work), (2) the average and standard deviation of the velocity magnitude at a height $Y = 40D$ (i.e. in the organized oscillation area) and the corresponding COV, (3) the same data for coordination number, and (4) the maximum velocity autocorrelation at $Y = 40D$ and the corresponding time-period (obtained in a manner similar to Fig. 6).

These results reveal that the flow rate through the hopper outlet is unaffected by the size distribution of the grains, as well as the average velocity in the organized oscillation area, while the average coordination number slightly increases with COV_D. The intensity of the instationarities (i.e. the coefficient of variation of these quantities) seems to decrease when increasing the dispersion of the grain sizes in the sample, but the coherence of the periodicity (quantified by the value of the maximum autocorrelation number) and their time-period do not seem to be modified by this parameter. Hence, polydispersity seems to limit the instationarities, but neither to change their nature nor to prevent them. Following this trend, we can however speculate that a very strongly polydisperse sample (e.g. with a fractal distribution) may only experience limited amount of flow oscillations, but it would have to be confirmed by further studies.

4.2 Influence of the hopper geometry

Figure 11 presents the influence of the diameter of the hopper outlet, with values varying from $6D$ to $14D$ (all the other parameters being constant and equal to those of the reference experiment). Flow rate and average velocity both increase quite strongly with the outlet diameter, as predicted by Beverloo law, and the average coordination number is rather small (3.3–3.4) for intermediate values of the outlet diameter ($8 - 10D$) but larger (3.8–4.2) for extreme values.

We find the same kind of trend when analyzing the intensity of the instationarities (COV of velocity and

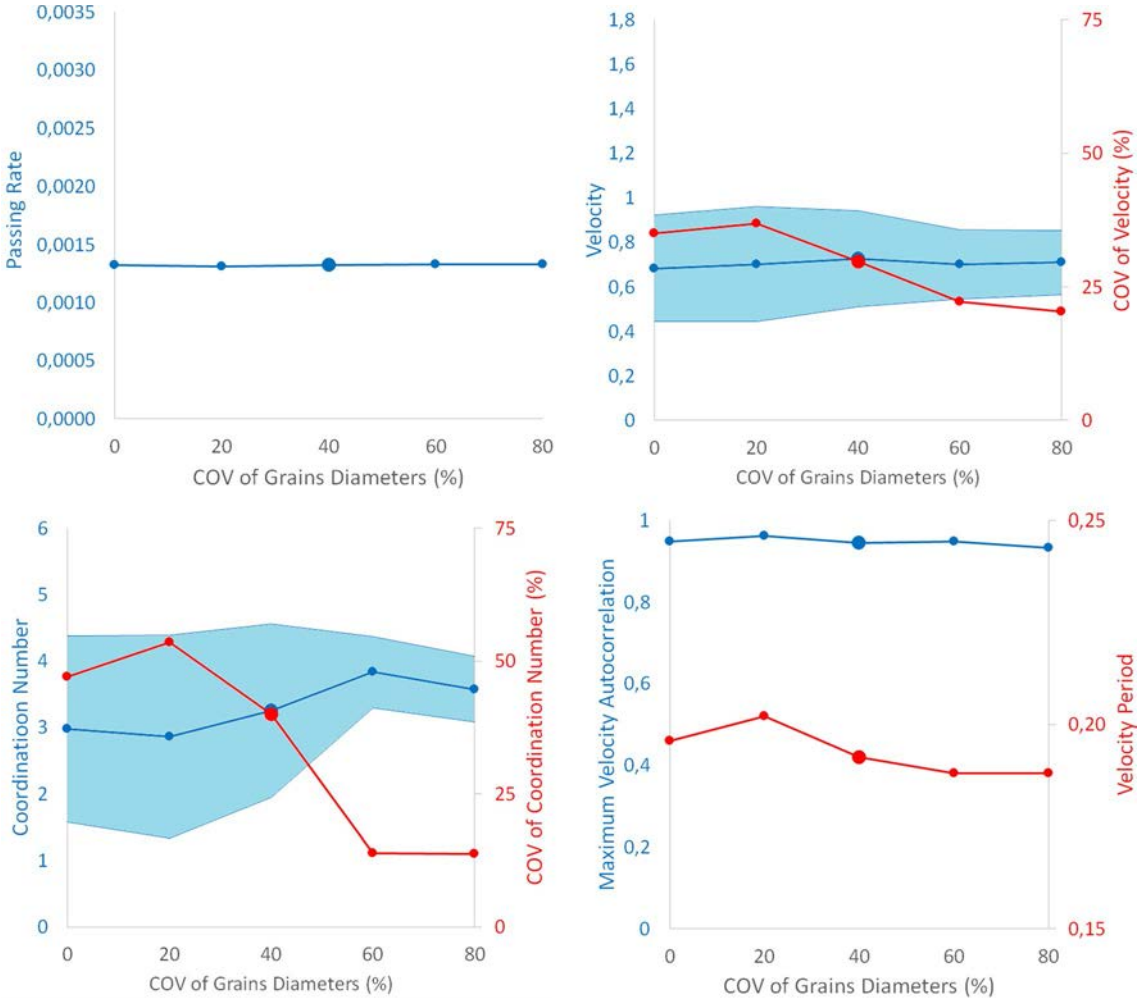

Fig. 10 Influence of the coefficient of variation of D; upper-left: discharge rate; upper-right: velocity magnitude at $Y = 40D$ (mean value $\pm$ one SD), and corresponding coefficient of variation; lower-left: same plot for coordination number; lower-right: value of the maximum autocorrelation of the velocity signal, and time-period corresponding to this maximum value

coordination number), the quality of their periodicity structure (maximum autocorrelation value) and their time-period. It is clear that hopper outlet diameters of $8 - 10D$ favor the appearance and development of the organized flow fluctuations. For these simulations, the instationarities are more intense (with coefficients of variation of 30–50% for velocity and 30–40% for coordination number), and with clearer patterns (maximum autocorrelation close to 1), with a constant period. In contrast, when considering very small ($6D$) or large ($\geq 12D$) outlet diameters, the oscillations get less intense and with a much less clear periodicity. This is especially the case for large diameters, with coefficients of variation smaller than 10% for the velocity and the coordination number, a maximum autocorrelation lower than 0.8 (and as low as 0.5 in the case of $14D$), and a decreasing time-period. It is likely that considering even larger outlet diameters would lead these organized fluctuations to vanish.

The influence of the hopper opening angle is presented in Fig. 12, from the case of a very flat hopper (angle to the horizontal $\alpha = 40°$) to a very steep one ($\alpha = 80°$). Since the general geometry of the hopper changes in each simulation, local quantities (i.e. mean and standard deviation of velocity and coordination number) are computed at a varying height located $10D$ below the free surface at the hopper inlet, which corresponds to the location where organized fluctuations are the most prone to be observed. Figure 12 reveals that steep hoppers tend to increase the flow rate, but that fluctuations are favored by intermediate values of the opening angle. Flat hoppers ($\alpha = 40 - 50°$) indeed lead to very limited instationarities (COV smaller that 8% for velocity and coordination number) with a much less clear periodic structure. The case $\alpha = 40°$ even leads to a complete disappearance of any kind of periodic fluctuations of the flow parameters. Similar observations are made for the steepest case ($\alpha = 80°$). It is nevertheless interesting to observe that the shape of the

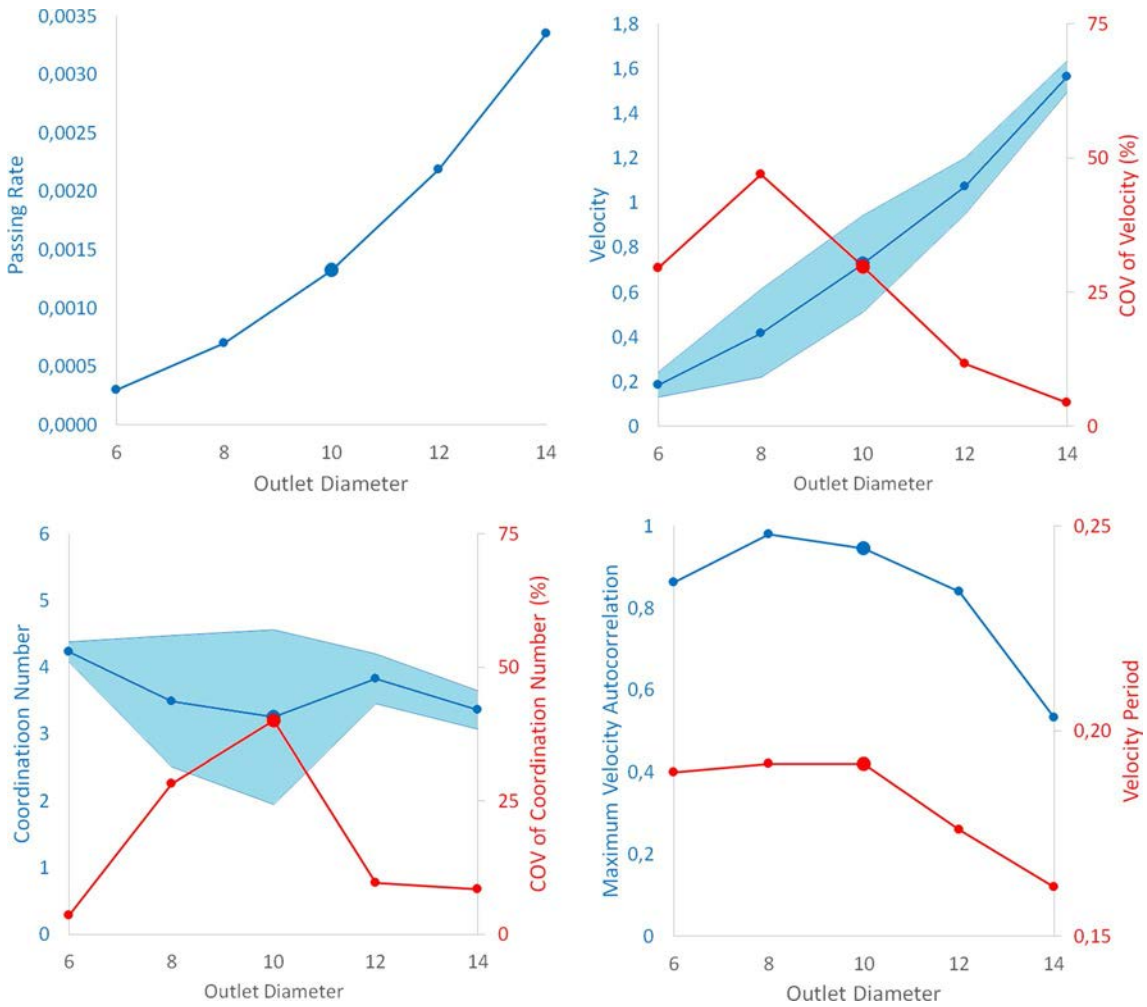

Fig. 11 Influence of the outlet diameter; upper-left: discharge rate; upper-right: velocity magnitude at $Y = 40D$ (mean value $\pm$ one SD), and corresponding coefficient of variation; lower-left: same plot for coordination number; lower-right: value of the maximum autocorrelation of the velocity signal, and time-period corresponding to this maximum value

hopper has a systematic influence on the time-period of the oscillations, with periods strongly increasing with the hopper angle.

4.3 Influence of the contact model

In a preliminary study performed in the same numerical framework [22], the effect of the contact stiffness $k_n = k_t$ was investigated. It was found that this parameter did not have any influence on the discharge rate, but that the periodicity of the flow oscillations was proportional to the inverse square root of this stiffness. It clearly indicated that the development of such oscillations relied on the elasticity of the contacts between the grains.

In this paragraph, we evaluate the influence of the two other parameters of the standard contact model of DEM: friction and damping coefficients. Figure 13 presents numerical results obtained for friction coefficients varying from $\mu = 0.0$ to $\mu = 0.8$. The hopper discharge rate slightly decreases with an increasing friction, as well as the average velocity and coordination number. There is however a clear change of oscillation regime between low and high friction values. For friction coefficients lower than 0.4, instationarities are very faint (coefficients of variation close to 5% for velocity and coordination number) and only poorly periodic. In the case of a null friction, the periodic structure completely vanishes. For larger friction coefficients, however, the intensity and coherence of the oscillations are high and rather constant. It is interesting to notice that large friction coefficients lead to larger time periods of the oscillations.

The influence of the damping coefficient is detailed in Fig. 14, for damping values ranging from $\gamma = 0.0$ to $\gamma = 0.4$ (a value of 1.0 corresponding to critical damping). It appears that the influence of this parameter on the system is rather limited, except for a decrease of the intensity of the coordination number oscillations with a larger damping. For all the

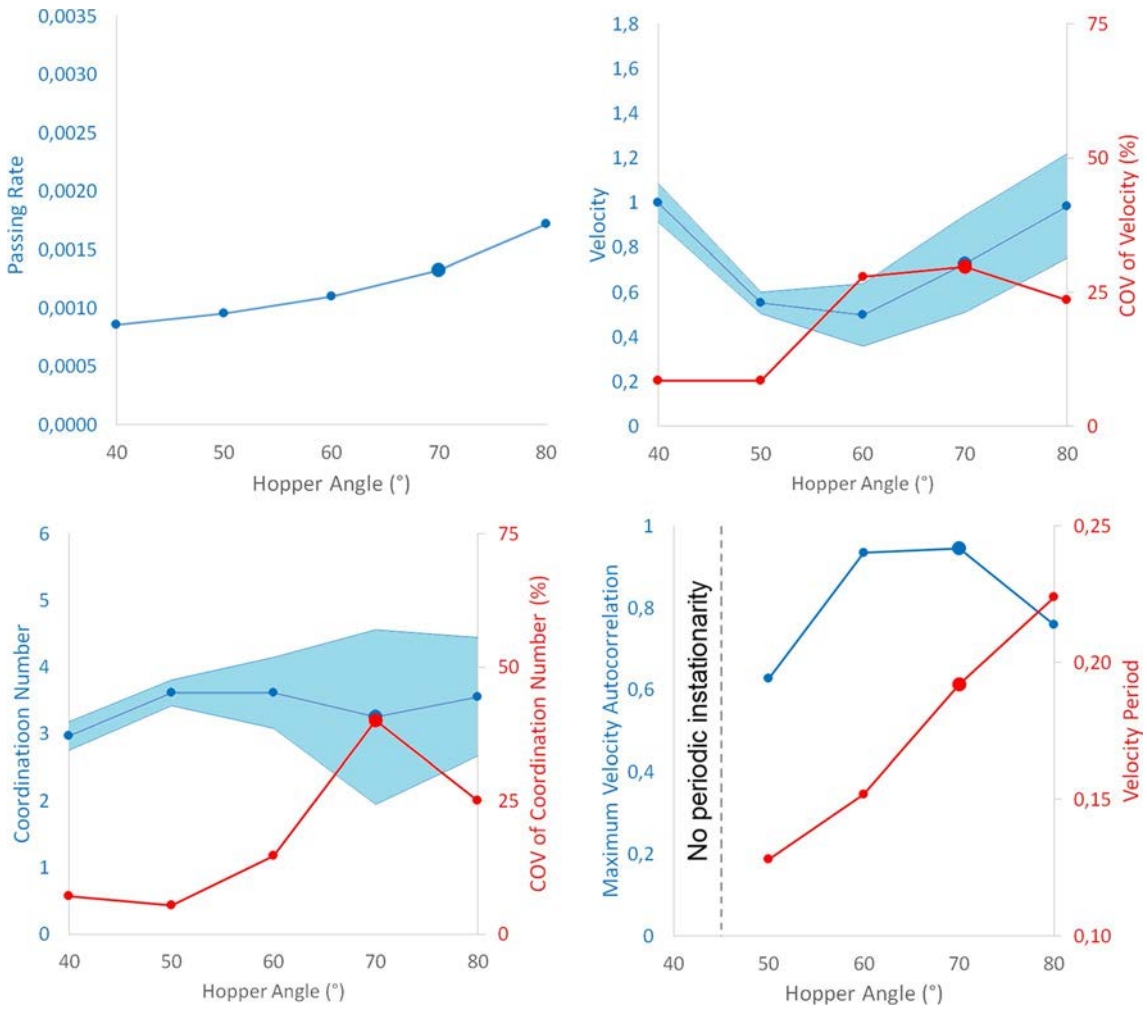

Fig. 12 Influence of the hopper angle; upper-left: discharge rate; upper-right: velocity magnitude at a distance of 10 below the hopper inlet (mean value ± one SD), and corresponding coefficient of variation; lower-left: same plot for coordination number; lower-right: value of the maximum autocorrelation of the velocity signal, and time-period corresponding to this maximum value

values of γ, the periodic structure of the oscillations remains very clear (autocorrelation close to 1), and the main period remains unmodified.

5 Discussion and conclusion

The observations gathered during this numerical campaign reveal that 3D granular hopper flows are very prone to organized instationarities. They appear to occur as intense variations of the velocity field and of the contact structure of the granular sample, which are chaotic in the neighborhood of the hopper outlet but gain a clear periodicity and structure above a certain height. They take the shape of rapidly propagating waves originating from the hopper outlet and lateral walls and propagating upwards and inwards, leading to almost synchronized oscillations of the flow parameters in the upper part of the hopper. While velocity variations are quasi-harmonic, variations in the coordination number are more skewed, with short events of important contacts loss followed by longer stages of reconstruction of the contact network. The granular density of the sample, represented here by the solid fraction, is only submitted to very limited variations in amplitude, but can nevertheless be detected by appropriate procedures and appear to be perfectly in phase with the coordination number signal.

The time delay between the velocity and coordination number variations and the propagation patterns of the waves transporting them draw a general pictures of the instationarities that follow several successive stages:

1. Force chains build up from the hopper outlet and from its lateral walls, because of the converging character of the flow. This leads to an increase in the coordination num-

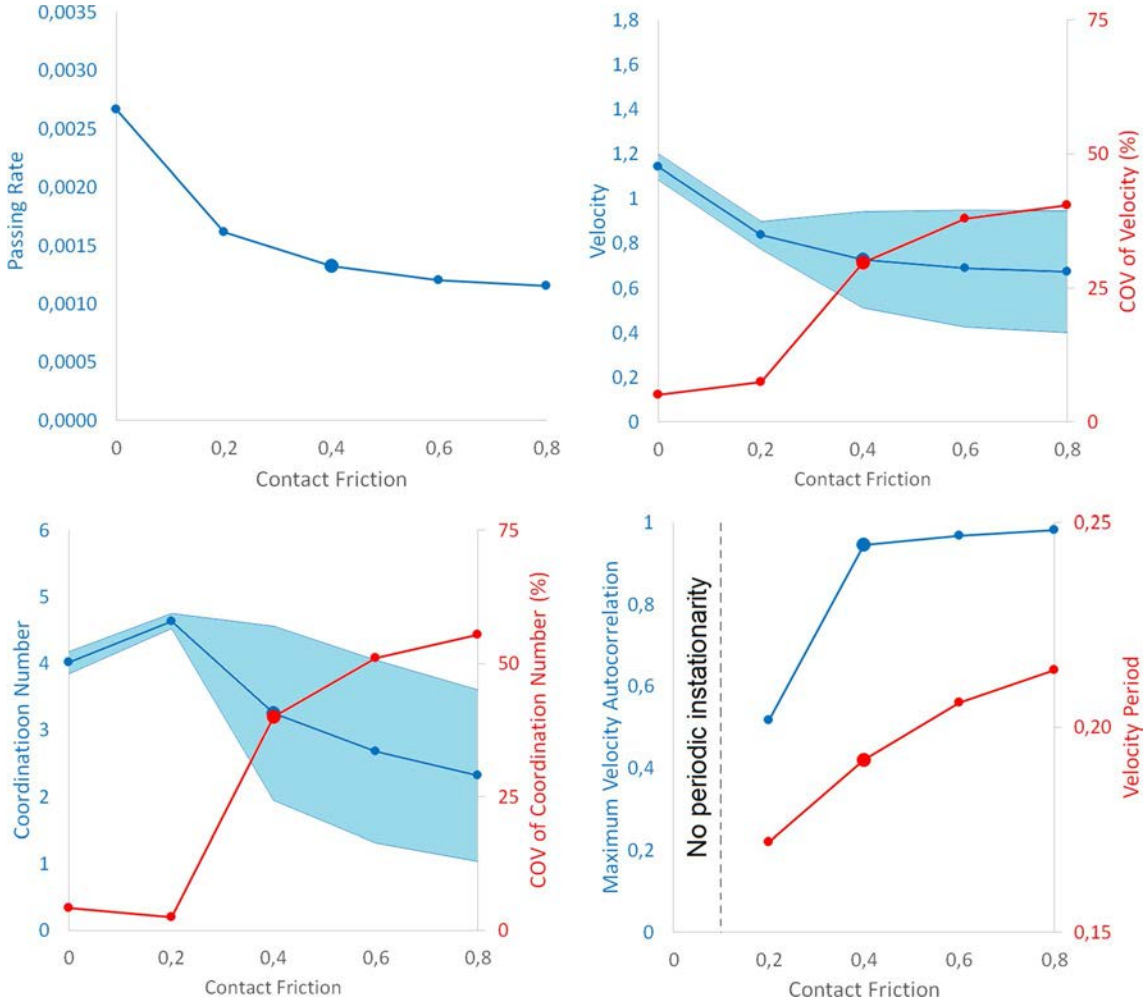

Fig. 13 Influence of the contact friction coefficient; upper-left: discharge rate; upper-right: velocity magnitude at $Y = 40D$ (mean value $\pm$ one SD), and corresponding coefficient of variation; lower-left: same plot for coordination number; lower-right: value of the maximum autocorrelation of the velocity signal, and time-period corresponding to this maximum value

ber and in the solid fraction, which propagate upwards and inwards. The force chains emanating from the lateral walls meet in the central area of the hopper.

2. Because of this stronger confinement grains velocities decrease while coordination number stabilizes at a value close to one standard deviation above its average.
3. These patterns, limited in amplitude close to the walls, reach the central area of the hopper where they acquire their maximum amplitude. Velocity reaches a minimum, while the flow of the matter below continues, leading to a progressive decrease in the local confinement: coordination number starts to decrease.
4. Solid fraction reaches a minimum and, while the amplitude of this variation is very small, it translates into a strong drop in the coordination number (two standard deviations below its average) which favors an acceleration of the flow. Velocity increases.
5. This velocity increase finally leads to a reconstruction of the contact network and a new increase of the granular density and of the coordination number. Velocities reach a maximum, first at the outlet and close to the lateral walls, and then in the central and upper parts of the hopper. The cycle continues.

The systematic parametric study described in Sect. 4 suggests that some specific conditions are necessary for the initiation and continuance of such organized and periodic instationarities. A specific range of hopper outlet diameter (between $8D$ and $10D$) and of hopper opening angle (between 60° and 70° with the horizontal) are needed, otherwise the fluctuations do not gain intensity and periodic structure. A minimum value of the coefficient of friction of 0.4 is also necessary. The polydispersity of

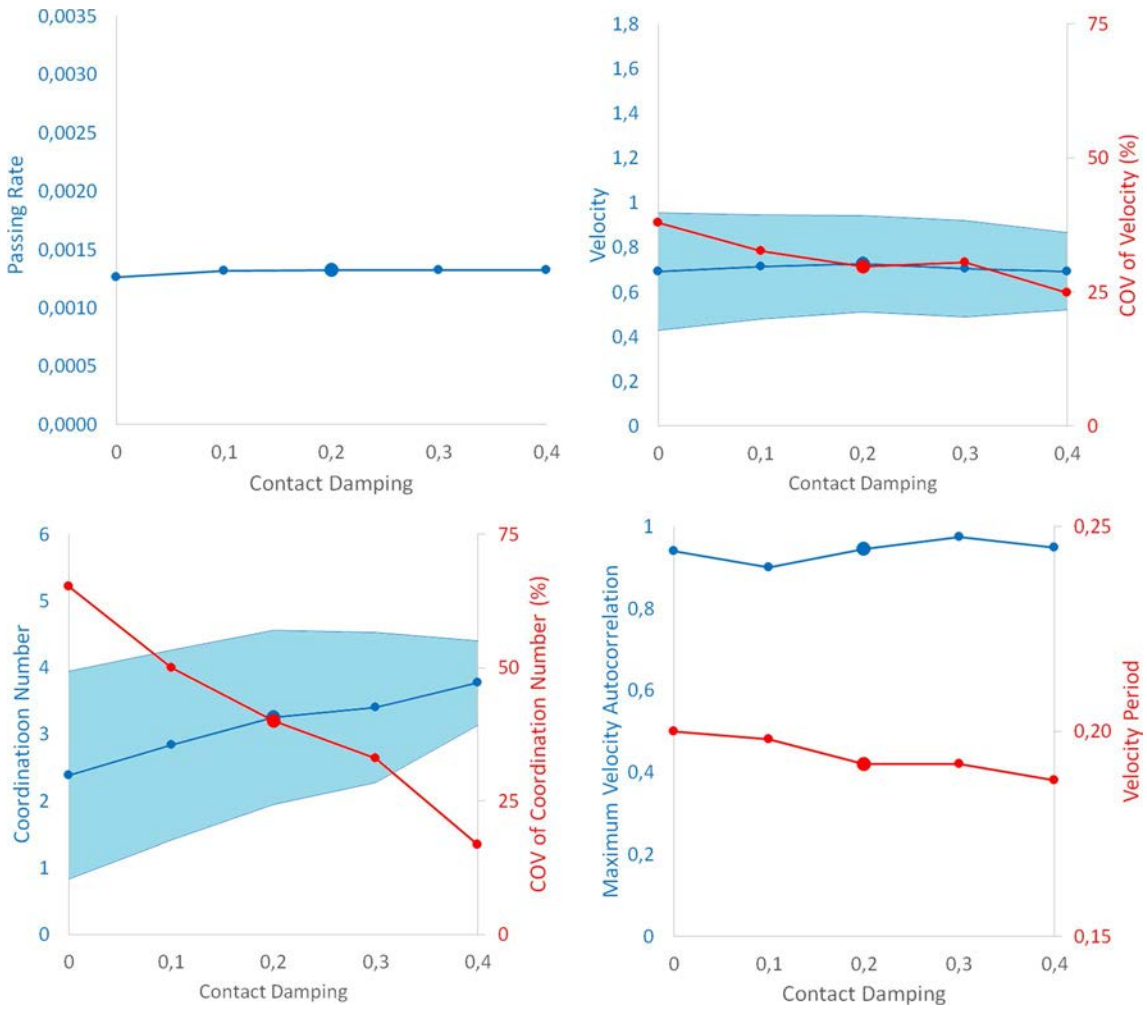

Fig. 14 Influence of the contact damping coefficient; upper-left: discharge rate; upper-right: velocity magnitude at $Y = 40D$ (mean value $\pm$ one SD), and corresponding coefficient of variation; lower-left: same plot for coordination number; lower-right: value of the maximum autocorrelation of the velocity signal, and time-period corresponding to this maximum value

the sample and the contact damping do not seem to have any major effect, on the other hand.

The reasons for these restricted conditions are still unclear, in particular because there is no apparent correlation between the discharge rate and the properties of the instationarities. For example, the change of oscillation regime is very clear between the cases $\mu = 0.2$ and $\mu = 0.4$ (Fig. 13), but no such drastic change is observed in terms of the discharge rate, which follows the same trend as for larger values of μ. Hence, a simplistic explanation relating the appearance of the fluctuations to the larger difficulty of the grains to flow through the hopper (which would lead them to collide more and would induce vibrations) does not seem to hold. Same observations can be made for the hopper outlet diameter and opening angle.

This is confirmed by Fig. 15, which shows vertical profiles of the coefficient of variation of the velocity magnitude and of the coordination number along the revolution axis of the hopper, for the reference simulation, for the case of a hopper opening diameter of $6D$, and for the case of a friction angle of $\mu = 0.2$. It clearly appears that the behaviors of these three systems in terms of flow variability are very similar in the lower part of the hopper, i.e. below a height of $10 - 15D$. It is only above this height that the reference simulation starts to exhibit more intense instationarities, while the other two simulations do not. It would thus appear that organized fluctuations are not related to phenomena occurring in the close neighborhood of the outlet, such as the collisional regime transition. It can be speculated that their ability to self-organize may result from a complex interplay between the hopper geometry and the ability of the granular material (enhanced by a higher contact friction) to form strong and persistent force chains and thus to coordinate grains motions on a longer range. This interplay is yet to be

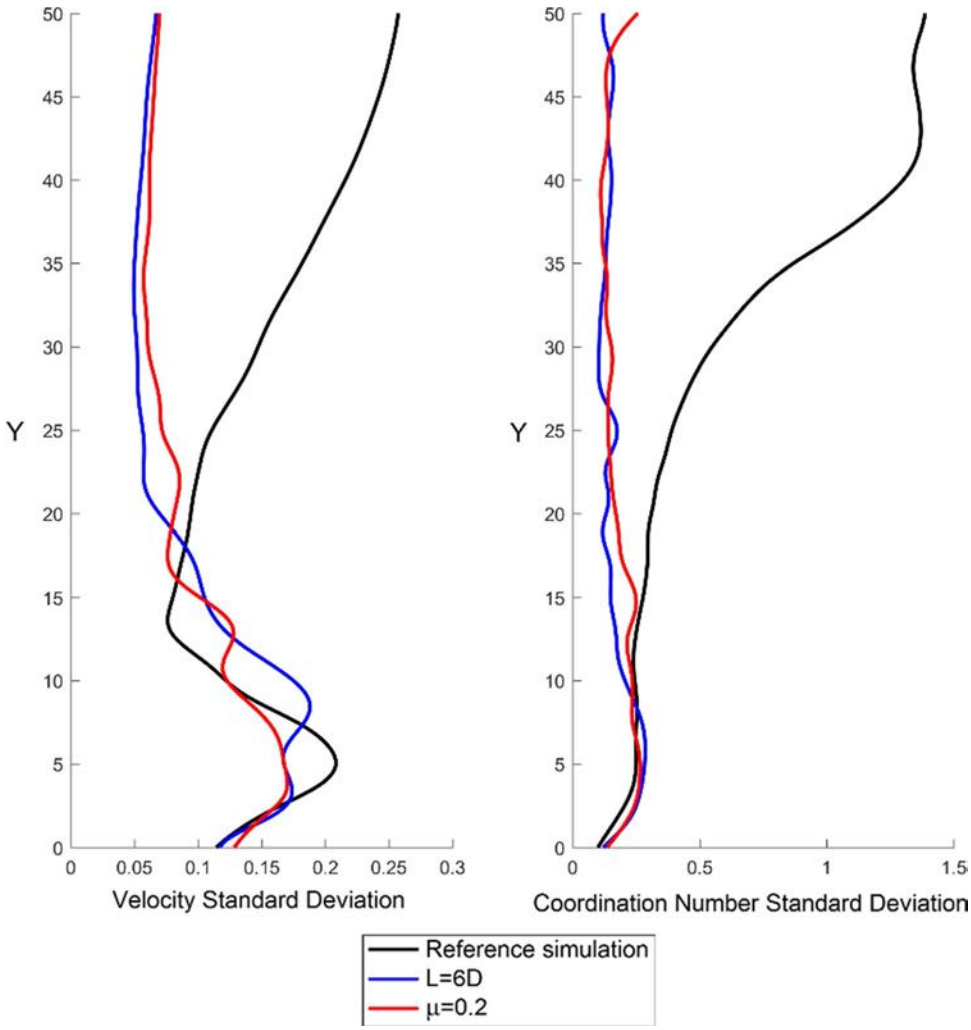

Fig. 15 Standard deviations of velocity and coordination number as functions of the location Y on the revolution axis of the hopper, for the reference simulation, the case of an opening diameter of $6D$, and the case of a friction coefficient $\mu = 0.2$

understood. Further studies will focus on this assumption, and will explore the implications of a more realistic (i.e. non-linear) contact stiffness, of larger polydispersity, and of more complex grains shapes [34].

References

1. Forterre, Y., Pouliquen, O.: Flows of dense granular media. Annu. Rev. Fluid Mech. **40**, 1–24 (2008)
2. Cleary, P.W., Sawley, M.L.: DEM modelling of industrial granular flows: 3D case studies and the effect of particle shape on hopper discharge. Appl. Math. Model. **26**, 89–111 (2002)
3. Wan, J.F., Zhang, S., Tian, Y., Lin, P., Yang, G., Yang, L.: Influence of geometrical and material parameters on flow rate in simplified ADS dense granular-flow target: a preliminary study. J. Nucl. Sci. Technol. **53**(11), 1809–1815 (2016)
4. Jia, X., Gui, N., Yang, X., Tu, J., Jiang, S.: Fluctuation and arching formation of very dense and slow pebble flow in a silo bed. J. Nucl. Sci. Technol. **54**(1), 111–126 (2017)
5. Pizette, P., Govender, N., Wilke, D.N., Abriak, N.E.: DEM GPU studies of industrial scle particle simulations for granular flow civil engineering applications. EPJ Web Conf. **140**, 03071 (2017)
6. Nguyen, T.V., Brennen, C., Sabersky, R.H.: Gravity flow of granular materials in conical hoppers. J. Appl. Mech. **46**, 529–535 (1979)
7. Bazant, M.Z.: A theory of cooperative diffusion in dense granular flows (2004). arXiv:cond-mat/0307379v2
8. . Hendy, S.: Instabilities in granular flows (2008). arXiv:cond-mat/0007236v1
9. Sun, J., Sundaresan, S.: Radial hopper flow prediction using constitutive model with microstructure evolution (2012). arXiv :1207.1751v1
10. Michalowski, R.L.: Flow of granular material through a plane hopper. Powder Technol. **39**, 29–40 (1983)
11. Baxter, G.W., Behringer, R.P., Fagert, T., Johnson, G.A.: Pattern formation in flowing sand. Phys. Rev. Lett. **62**(24), 2825–2828 (1989)
12. Choi, J., Kudrolli, A., Bazant, M.Z.: Velocity profile of granular flows inside silos and hoppers. J. Phys.: Condens. Matter **17**, S2533–S2548 (2005)
13. Gardel, E., Keene, E., Dragulin, S., Easwar, N., Menon, N.: Force-velocity correlations in a dense, collisional, granular flow (2006). arXiv:cond-mat/0601022
14. Gardel, E., Seitaridou, E., Facto, K., Keene, E., Hattam, K., Easwar, N., Menon, N.: Dynamical fluctuations in dense granular flows. Philos. Trans. R. Soc. A **367**, 5109–5121 (2009)

15. Gentzler, M., Tardos, G.I.: Measurement of velocity and density profiles in discharging conical hoppers by NMR imaging. Chem. Eng. Sci. **64**, 4463–4469 (2009)
16. Vivanco, F., Rica, S., Melo, F.: Dynamical arching in a two dimensional granular flow. Granular Matter **14**(5), 563–576 (2012)
17. Villagran Olivares, M.C., Benito, J.G., Uñac, R.O., Vidales, A.M.: Towards a one parameter equation for a silo discharging model with inclined outlets. Powder Technol. **336**, 265–272 (2018)
18. Ristow, G.H., Herrmann, H.J.: Density patterns in two-dimensional hoppers. Phys. Rev. E **50**(1), R5–R8 (1994)
19. Potapov, A., Campbel, C.S.: Computer simulation of hopper flow. Phys. Fluids **8**(11), 2884–2894 (1996)
20. Mollon, G., Zhao, J.: Characterization of fluctuations in granular hopper flow. Granular Matter **15**(6), 827–840 (2013)
21. Magalhães, F.G.R., Atman, A.P.F., Moreira, J.G., Herrmann, H.J.: Analysis of the velocity field of granular hopper flow. Granular Matter **18**, 33 (2016)
22. Mollon, G., Zhao, J.: Granular flow fluctuations in a conical hopper. Powders and Grains 2017, 3–7 July 2017, Montpellier, France, EPJ Web of Conferences, vol 140, p. 03030 (2017)
23. Wang, N., Xu, J., Guo, X., Lu, H., Zhao, H., Li, W., Liu, H.: Velocity profiles of avalanches during hopper discharge. Fuel **218**, 350–356 (2018)
24. Guo, Z., Chen, X., Xu, Y., Liu, H.: Enhancing the linear flow of fine granules through the addition of elongated particles. Sci. Rep. **5**, 16071 (2015)
25. Szabo, B., Kovacs, Z., Wegner, S., Ashour, A., Fischer, D., Stannarius, R., Börzsönyi, T.: Flow of anisometric particles in a quasi-two-dimensional hopper. Phys. Rev. E **97**, 062904 (2018)
26. Tang, J., Behringer, R.P.: How granular materials jam in a hopper. Chaos **21**, 041107 (2011)
27. Cundall, P.A., Strack, O.D.L.: A discrete numerical model for granular assemblies. Geotechnique **29**, 47–65 (1979)
28. Mollon, G., Richefeu, V., Villard, P., Daudon, D.: Discrete modelling of rock avalanches: sensitivity to block and slope geometries. Granular Matter **17**(5), 645–666 (2016)
29. Mollon, G.: A numerical framework for discrete modelling of friction and wear using Voronoi polyhedrons. Tribol. Int. **90**, 343–355 (2015)
30. Goldhirsch, I.: Stress, stress asymmetry and couple stress: from discrete particles to continuous fields. Granular Matter **12**, 239–252 (2010)
31. Weinhart, T., Thornton, A.R., Luding, S., Bokhove, O.: Closure relations for shallow granular flows from particle simulations. Granular Matter **14**, 531–552 (2012)
32. Fasshauer, G.E.: Meshfree approximation methods with matlab. World Scientific, ISSN 1793-1355 (2007)
33. Grigoli, F., Cesca, S., Krieger, L., Kriegerowski, M., Gammaldi, S., Horalek, J., Priolo, E., Dahm, T.: Automated microseismic event location using master-event waveform stacking. Sci. Rep. **6**, 25744 (2016)
34. Mollon, G., Zhao, J.: 3D generation of realistic granular samples based on random fields theory and Fourier shape descriptors. Comput. Methods Appl. Mech. Eng. **279**, 46–65 (2014)